

## Geochemistry in the lung: Reaction-path modeling and experimental examination of rock-forming minerals under physiologic conditions†

ANNE E. TAUNTON,<sup>1</sup> MICKEY E. GUNTER,<sup>1,2,\*</sup> GREGORY K. DRUSCHEL,<sup>3</sup> AND SCOTT A. WOOD<sup>1</sup>

<sup>1</sup>Department of Geological Sciences, University of Idaho, Moscow, Idaho 83844, U.S.A.

<sup>2</sup>Marsh Professor-at-Large, University of Vermont, Burlington, Vermont 05405, U.S.A.

<sup>3</sup>Department of Geology, University of Vermont, Burlington, Vermont 05405, U.S.A.

### ABSTRACT

A novel and promising application of a geochemical tool adapted to medical science is the thermodynamic and kinetic modeling of the behavior of minerals in fluids similar to lung fluids (or simulated lung fluids, SLF). Reaction-path modeling for chrysotile, anorthite, K-feldspar, talc, muscovite, kaolinite, albite, and quartz under physiologic conditions in SLF gives dissolution times for these minerals as: chrysotile < anorthite < K-feldspar < talc < muscovite = kaolinite = albite = quartz. For the reaction of these minerals with SLF, hydroxylapatite (a mineral initially supersaturated in SLF) and several other secondary minerals were predicted to form (e.g., mesolite is predicted to precipitate during dissolution reactions of other Al<sup>3+</sup>-containing minerals). Batch experiments using SLF and a brucite/chrysotile mineral mixture confirm that hydroxylapatite forms during reactions in SLF, potentially a function of having a seed crystal in the brucite, chrysotile, or hydromagnesite (predicted to form from brucite dissolution) present. Moreover, SEM analysis of lung tissue also confirms the formation of calcium phosphates (e.g., hydroxylapatite). Reaction-path modeling of minerals under physiologic conditions provides insight into mineral behavior in the body; predicted mineralization pathways associated with pleural plaques and the predicted formation of Al<sup>3+</sup>-bearing minerals during reaction-path modeling deserve attention when considering pathologies in the body.

**Keywords:** Medical mineralogy, mineral dissolution, Geochemist workbench, reaction-path modeling, lung mineralogy

### INTRODUCTION

Although minerals and poorly crystalline inorganic particles with compositions similar to minerals commonly form in the human body, geoscientists are not typically involved in their study. Bones and teeth are constructed and deconstructed daily in the presence of physiologic fluids, and this process is well researched and documented (e.g., Skinner 2005; Glimcher 2006; and references therein). Pathologic minerals precipitated within the body such as gallstones, kidney stones, and tissue calcifications are not uncommon, with gallstones affecting up to 20% of the population, and kidney stones affecting up to 5% (McCance and Huether 2002). The geologic community is recognizing that geochemical techniques used to predict, identify, and quantify minerals in low-temperature aqueous environments such as surface waters can be adapted to and useful in other low-temperature environments, namely the human body.

Medical geology is a relatively new concept, but geologists have been aiding the regulatory and health-care communities for several decades (e.g., Guthrie and Mossman 1993). Over the past 10 years, several geologic conferences have focused on this increasingly recognized subfield of geology, and with each conference, geologists and other researchers identify more research topics

and adapt various techniques, continuing to merge the health-care and geology fields. To that end, in 2005 the Geological Society of America established the Geology and Health division.

Humans are constantly inhaling and ingesting minerals. Most of these minerals are not pathologic, while others may cause disease. What makes one mineral pathologic and another not? Dose, mineral size, density, morphology, crystallinity, dissolution kinetics, and chemical characteristics all can play a role in the pathologic effects of minerals (Plumlee et al. 2006; van Oss et al. 1999). Moreover, there is a distinction between toxicity and mutagenicity of a mineral (Davis 2001). A toxic mineral is one that destroys cells and causes an inflammatory response in the body, and in the lung often causing a fibrosis. As an example, both asbestos and quartz can be toxic leading to asbestosis and silicosis, respectively, if the doses are high enough. Gunter (1999) provides an overview of health issues associated with quartz inhalation and Norton and Gunter (1999) discuss relationships between quartz-rich PM10 and respiratory diseases in Idaho. Mutagenic or neoplastic behavior refers to the ability of a mineral to actually disrupt the normal cell replication process, which may lead to cancer. Amphibole asbestos such as crocidolite, for example, has been associated with mesothelioma, a type of cancer that is associated with amphibole asbestos exposure (McDonald and McDonald 1997); also see Gunter et al. (2007a) for a discussion on amphibole exposure and health issues. Understanding the specific physiological reactions that cause these effects is an active area of research and another way mineralogy and

\* E-mail: mgunter@uidaho.edu

† Open Access, thanks to the author's funding. Article available to all readers via GSW (<http://ammin.geoscienceworld.org>) or the MSA website.

geochemistry may provide valuable insight. For example, some mineral surfaces are known to generate free radicals at defects and electron hole-pair sites that may be an avenue of significant cellular destruction (Borda et al. 2003; Cohn et al. 2006; Dutta and Moudgil 2007).

Reaction-path modeling is a tool used by aqueous geochemists to predict the behavior of minerals in a particular fluid. Models can be developed for closed or open environments with a specified primary fluid composition and, if desired, a secondary fluid that flushes through the system at designated points of time. Reaction-path modeling was used by Wood et al. (2006) to predict the behavior of tremolite and chrysotile in simulated lung fluids. The present paper reports reaction-path modeling of the interaction of selected rock-forming minerals with simulated lung fluid (SLF) and considers the geochemical properties of these minerals in the body. Aqueous batch experiments and scanning electron microscope (SEM) analysis of calcified pleural plaques confirm the modeling prediction of the precipitation of calcium phosphate particles in the lung from a simulated lung fluid composition that is initially supersaturated with respect to hydroxylapatite.

## EXPERIMENTAL METHODS

### Reaction-path modeling

For this project, modeling of the dissolution reactions of single minerals (as opposed to mixtures of minerals) was performed as a first step toward understanding dissolution processes under simulated lung conditions. Eleven rock-forming minerals (Table 1) were initially considered for reaction-path modeling under physiologic conditions. These minerals were chosen because of their predominance in the environment and/or their use in industry. However, efforts to model tremolite and diopside flushed with lung fluid at pH 7.4 were unsuccessful (multiple attempts to do this with the approaches outlined below did not numerically converge to a solution) and therefore are not included in the results.

The Geochemist's Workbench (GWB) (Bethke 1996) and a thermodynamic database (thermo.com.v8.r6+.dat) included with the package were used for our calculations. Thermodynamic data for struvite,  $\text{MgNH}_4\text{PO}_4$ , were added to this database for use in these calculations as this mineral has been found to be a potentially important biomineral in human systems (Aage et al. 1997; Kofina and Koutsoukos 2005; Bhuiyan et al. 2007). This geochemical modeling program allows the user to simulate mineral dissolution in many different fluid types and predict the precipitation of secondary minerals over time. Previous research on the behavior of chrysotile and tremolite asbestos, two asbestiform minerals important to public health (Wood et al. 2006), provides a detailed description of the tools used in this paper. The minerals and the rate constants used for modeling are listed in Table 1. With the exception of calcite, all minerals were silicates.

Dissolution rates for silicate minerals in neutral pH solutions are often expressed as variable order with respect to  $\text{H}^+$  (Drever 1994; Lasaga et al. 1994), dependent on the specific area of wetted surface,  $A_w$  (Paces 1983; Langmuir 1997) and vary as a function of approach to equilibrium expressed as the saturation index  $\left(\frac{Q}{K_{\text{eq}}} - 1\right)$  (Langmuir 1997)

**TABLE 1.** Rate constants for minerals employed in reaction-path modeling using "The Geochemists Workbench"

Mineral	Rate constant (mol/cm <sup>2</sup> ·s)	Reference
Calcite	$1.00 \times 10^{-10}$	Chou et al. (1989)
Chrysotile	$5.9 \times 10^{-14}$	Jurinski and Rimstidt (2001)
K-feldspar	$1.00 \times 10^{-14}$	Est. from Blum and Stillings (1995)
Anorthite	$1.00 \times 10^{-14}$	Est. from Blum and Stillings (1995)
Talc	$1.40 \times 10^{-15}$	Jurinski and Rimstidt (2001)
Muscovite	$2.51 \times 10^{-17}$	Est. from Nagy (1995)
Kaolinite	$5.01 \times 10^{-17}$	Carroll and Walther (1990)
Albite	$1.00 \times 10^{-16}$	Est. from Blum and Stillings (1995)
Quartz	$1.40 \times 10^{-17}$	Jurinski and Rimstidt (2001)
Tremolite	$1.00 \times 10^{-16}$	Wood et al. (2006)
Diopside	$2.88 \times 10^{-14}$	Knauss et al. (1993)

$$\text{rate} = k a_{\text{H}^+} A_w \left( \frac{Q}{K_{\text{eq}}} - 1 \right) \quad (1)$$

where,  $k$  is the rate constant and  $a_{\text{H}^+}$  is the activity of  $\text{H}^+$ . At near-neutral pH (i.e., physiologic pH), the rate law becomes zero-order with respect to hydrogen-ion activity leaving the rate constant ( $k$ ) of the dissolution reaction equal to the rate of the reaction divided by the surface area at near-neutral pH and far from equilibrium (Blum and Stillings 1995; Hellmann 1994).

In the presence of organic acids, dissolution rates for silicates generally increase (Cama and Ganor 2006; Golubev and Pokrovsky 2006; Welch and Ullman 2000; Blum and Stillings 1995). Unfortunately, thermodynamic and kinetic data for all possible organic complexes involved in the dissolution of minerals in the body do not exist. One can extrapolate, however, from previous laboratory and field research, that the presence of organic acids in the body will increase the rates of mineral dissolution under physiologic conditions. As well, the intracellular pH of a macrophage, one of the cellular defenses to foreign particles in the lungs, is 4.5 (Plumlee et al. 2006), so we can expect the rate of dissolution also to increase if the mineral is engulfed by a macrophage. Enzymatic effects on dissolution rates (potentially resulting in an increase or decrease in overall dissolution rates) should also be considered to more fully describe the reactions governing mineral dissolution in the body. The current work uses existing thermodynamic and kinetic data to constrain possible mineralization processes in SLF; clearly there are additional complexities to consider and a need for better data, but that is outside the scope of this work.

The Geochemist's Workbench uses a kinetic dissolution model based on total surface area, rate constant, and solution saturation state. The model is defined as

$$\text{rate} = A_s k_+ \left( \frac{Q}{K_{\text{eq}}} - 1 \right) \quad (2)$$

where,  $A_s$  is the total surface area (determined from the mass of the mineral present and a surface area per mass term),  $k_+$  is the rate constant for the forward reaction (dissolution) at constant pH,  $Q$  is the ion activity product for the dissolution reaction, and  $K_{\text{eq}}$  is the equilibrium constant for the dissolution reaction. The term

$$\left( \frac{Q}{K_{\text{eq}}} - 1 \right)$$

indicates the state of solution saturation with respect to the dissolving mineral phase.

Surface-area calculations were based on mineral morphology and particle density estimates for lung tissue of people exposed to occupational and environmental doses. Two different morphologies were used: a sphere and a rectangular prism representing the 3:1 aspect ratio commonly used by regulatory agencies when counting fibers in an occupational setting. These morphologies approximate the two most common morphologies of the minerals in this project. Surface area constraints for minerals in The Geochemist's Workbench must be normalized to mass (cm<sup>2</sup>/g). Therefore, to determine the surface area of a mineral per unit mass in the lung, the surface area of a single crystal was divided by the volume of the crystal and the particle densities. For the sphere morphology, the simplified equation is

$$SA_{\text{sphere}} = \frac{3}{r\rho} \quad (3)$$

where  $r$  is the radius and  $\rho$  is the mineral density. For a rectangular prism, the equation is

$$SA_{\text{rp}} = \frac{2/a + 2/b + 2/c}{\rho} \quad (4)$$

where,  $a$ ,  $b$ , and  $c$  are the length, width, and height of the prism, respectively, and  $\rho$  is the mineral density.

To illustrate the effects of surface area and dose on mineral dissolution and secondary mineral formation, models were constructed to represent both morphologies (sphere,  $s$ , and rectangular prism,  $rp$ ) across an order of magnitude in surface area (10000 and 100000 cm<sup>2</sup>/g), for mineral masses corresponding to environmental (25000 particles/mg dry lung) and occupational (300000 particles/mg dry lung) exposures. Chosen surface areas correspond to particle sizes of 0.2 and 2  $\mu\text{m}$  diameter spheres and  $0.2 \times 0.2 \times 0.6$  and  $2 \times 2 \times 6$   $\mu\text{m}$  rectangular prisms. Tables 2 and 3 list the total masses for fixed surface areas of 10000 and 100000

cm<sup>2</sup>/g based on these environmental and occupational exposures used as input for the geochemical modeling.

Blood plasma constantly exchanges components with cells of the lung and the surrounding extracellular fluid, and it is within this small volume of fluid between lung cells that inhaled minerals might react. The composition of extracellular lung fluid is assumed to be similar to blood plasma [though with lower concentrations of albumin, globulin, and fibronigen; Moss (1979); Kanapilly (1977); Mattson (1994)], and therefore the simulated lung fluid (SLF; Table 4) for these calculations is similar to that of blood plasma; we are however, modeling only the electrolyte composition of this fluid and not considering the organic ligands in this model. The composition of this SLF in this work is similar to those used in several other studies (Jurinski and Rimstidt 2001; Takaya et al. 2006; Sutton and Burastero 2003, 2004; Ford et al. 2008) (Table 5). This SLF is constrained to a fixed physiological pH (7.4) and a fixed  $P_{\text{CO}_2}$  fugacity (0.052) based on median values for healthy adults (Pagana and Pagana 2001). Additionally, an aluminum concentration of 370 nM was used, based on an upper limit of aluminum in blood plasma for healthy adults (Hewitt 1990), and a K<sup>+</sup> concentration of 0.004 M was used based on median values of for healthy adults (McCance and Huether 2002). It is of importance to note that some components reported for aqueous blood fluid composition do not differentiate between inorganic and organic sources. A critical example is for phosphorus; P can exist as phosphate (the PO<sub>4</sub><sup>3-</sup> ion and protonated forms) and as organic molecules, yet we are unaware of any analysis of blood plasma or lung fluids that may differentiate the phosphate-organic P content of the fluid. The level of phosphorus in SLF used in this study is also similar to levels of inorganic orthophosphate found in rat lung airway surface fluids (Govindaraju et al. 1997).

Nitrogen in these lung fluids was assumed to be present mainly as ammonia, 950 µg/L NH<sub>3</sub>, based on median values for healthy adults (Pagana and Pagana 2001), and was decoupled from nitrate in the model.

To simulate reasonable scenarios for the fate of minerals contained in lung tissue, several different models were used to illustrate potential mineral behavior, and several factors were varied over two orders of magnitude to highlight potential uncertainty regarding physical and physiological factors key to these mineral reactions. The model for mineral reactivity is based on the conceptual framework that a certain mass of a specific mineral (using 2 masses to represent median particle densities associated with occupational and environmental exposure; Tables 2 and 3) of a certain morphology (here comparing a spherical vs. a 3:1 aspect ratio shape) is in contact with a volume of lung fluid (10 mL) that is replaced over a certain time interval (this model looks at a 50 year residence time in lung tissue). The mineral in question will react with the lung fluid that is replaced with a volume of new, identical, “fresh” fluid in time steps; each step is a certain amount of time during which some of the mineral dissolves into the new fluid (based on an empirical dissolution rate), the ions from that dissolution combine with those in the lung fluid and precipitate minerals that are supersaturated. This can be done using a “flush” model design available in the GWB package, where each time step models how a new batch of fresh lung fluid (this fresh batch displaces the fluid from the prior step but leaves behind the minerals) interacts with the mineral of interest that is left and the secondary minerals deposited as a result of the prior step. This simulation in the GWB requires the mineral in question to constrain the concentration of a major ion (Bethke 1996) and a fluid of identical composition to the starting solution to be a reactant over these steps. The amount of fluid per day

**TABLE 2.** Total mineral mass for environmental (25 000 particles/mg dry lung) and occupational (300 000 particles/mg dry lung) exposures at constant surface area for spheres

Mineral	Sphere			
	SA = 10 000 cm <sup>2</sup> /g		SA = 100 000 cm <sup>2</sup> /g	
	Total mass (g) Environmental	Total mass (g) Occupational	Total mass (g) Environmental	Total mass (g) Occupational
Quartz	0.0161	0.193	1.61 × 10 <sup>-5</sup>	1.93 × 10 <sup>-4</sup>
Talc	0.0150	0.179	1.50 × 10 <sup>-5</sup>	1.79 × 10 <sup>-4</sup>
Kaolinite	0.0167	0.201	1.67 × 10 <sup>-5</sup>	2.01 × 10 <sup>-4</sup>
K-feldspar	0.0173	0.207	1.73 × 10 <sup>-5</sup>	2.07 × 10 <sup>-4</sup>
Calcite	0.0154	0.185	1.54 × 10 <sup>-5</sup>	1.85 × 10 <sup>-4</sup>
Albite	0.0165	0.198	1.65 × 10 <sup>-5</sup>	1.98 × 10 <sup>-4</sup>
Anorthite	0.0152	0.182	1.52 × 10 <sup>-5</sup>	1.82 × 10 <sup>-4</sup>
Muscovite	0.0142	0.171	1.42 × 10 <sup>-5</sup>	1.71 × 10 <sup>-4</sup>
Chrysotile	0.0177	0.212	1.77 × 10 <sup>-5</sup>	2.12 × 10 <sup>-4</sup>

**TABLE 3.** Total mineral mass for environmental (25 000 particles/mg dry lung) and occupational (300 000 particles/mg dry lung) exposures at constant surface area for rectangular prisms

Mineral	Rectangular prism			
	SA = 10 000 cm <sup>2</sup> /g		SA = 100 000 cm <sup>2</sup> /g	
	Total mass (g) Environmental	Total mass (g) Occupational	Total mass (g) Environmental	Total mass (g) Occupational
Quartz	0.0607	0.728	6.07 × 10 <sup>-5</sup>	7.28 × 10 <sup>-4</sup>
Talc	0.0563	0.676	5.63 × 10 <sup>-5</sup>	6.76 × 10 <sup>-4</sup>
Kaolinite	0.0630	0.756	6.30 × 10 <sup>-5</sup>	7.56 × 10 <sup>-4</sup>
K-feldspar	0.0650	0.780	6.50 × 10 <sup>-5</sup>	7.80 × 10 <sup>-4</sup>
Calcite	0.0580	0.696	5.80 × 10 <sup>-5</sup>	6.96 × 10 <sup>-4</sup>
Albite	0.0620	0.745	6.20 × 10 <sup>-5</sup>	7.45 × 10 <sup>-4</sup>
Anorthite	0.0571	0.686	5.71 × 10 <sup>-5</sup>	6.86 × 10 <sup>-4</sup>
Muscovite	0.0536	0.643	5.36 × 10 <sup>-5</sup>	6.43 × 10 <sup>-4</sup>
Chrysotile	0.0665	0.798	6.65 × 10 <sup>-5</sup>	7.98 × 10 <sup>-4</sup>

**TABLE 4.** Simulated lung fluid (SLF) composition used for modeling

Component	Concentration (mg/L)
Ca <sup>2+</sup>	0.00174
Cl <sup>-</sup>	0.115
CO <sub>2(g)</sub> fugacity	0.052
Mg <sup>2+</sup>	0.00104
Na <sup>+</sup>	0.145
HPO <sub>4</sub> <sup>2-</sup>	0.00104
SO <sub>4</sub> <sup>2-</sup>	0.000556
SiO <sub>2</sub> (aq)	0.00015
NH <sub>3</sub>	0.000053
Al <sup>3+</sup>	0.00000018
pH	7.4
Temperature (°C)	37

Note: Starting fluid composition supersaturated with respect to hydroxylapatite.

**TABLE 5.** Aqueous Gamble's solution (Jurinski and Rimstidt 2001)

Solvent	Concentration (mg/L)	Concentration (mg/L)
NaCl	6400	0.11
CaCl <sub>2</sub> ·2H <sub>2</sub> O	255	0.0045
MgCl <sub>2</sub> ·6H <sub>2</sub> O	212	0.0021
Na <sub>2</sub> SO <sub>4</sub> ·10H <sub>2</sub> O	179	0.00056
Na <sub>2</sub> HPO <sub>4</sub>	148	0.0010
NaHCO <sub>3</sub>	2700	0.032
Na <sub>2</sub> tartrate·2H <sub>2</sub> O	180	0.0013
Na <sub>3</sub> citrate·2H <sub>2</sub> O	153	0.00059
Na lactate (60% w/w)	290	0.0026
Glycine	118	0.0016
Na pyruvate	172	0.0015

(flush rate) can be changed by changing the amount of total fluid involved in each time step. Depending on the parameters (time, concentration, fluid volume, flush rate, mineral dissolution kinetics), there are hundreds to hundreds of thousands of steps in each simulation. Simpler, non-flush, modeling can also be accomplished for multiple minerals in a given fluid where a given mass of the mineral in question reacts with a fluid over time steps (this is analogous to a titration of the mineral into a set fluid volume), where each step sees a calculation of secondary mineral saturation, with the most supersaturated phases precipitating as secondary minerals at each step to attain equilibrium.

Previous research by Wood et al. (2006) using The Geochemist's Workbench demonstrated that both hydroxylapatite and ordered dolomite were predicted to form in physiologic reactions with tremolite and chrysotile asbestos. However, the authors concluded that dolomite was unlikely to form due to the difficulty of nucleating dolomite at low temperatures (Wood et al. 2006). Dolomite and other magnesium carbonates have been found in the body in rare occurrences as kidney stones (Mansfield 1980; Gault et al. 1993; Osbourne et al. 1986), but the amount of dolomite predicted to form during modeling is quite large. Similarly, even though Wood et al. (2006) demonstrated that quartz was predicted to form in tremolite reactions under physiologic conditions, they concluded that amorphous silica was the more likely phase to precipitate under these conditions. Due to these considerations, two different types of modeling were performed: modeling in which the precipitation of dolomite and quartz (and also magnesite) was suppressed (results presented in this paper) and modeling in which the precipitation of quartz and dolomite was allowed (Taunton 2007). Precipitation of secondary minerals was assumed to be instantaneous (i.e., because the kinetic factors of mineral precipitation under these conditions are unknown, it is assumed the minerals precipitate fast enough at these conditions to be modeled as instantaneous).

### Aqueous experiments

Batch experiments were conducted in 150 mL polyethylene bottles. The physiologic simulated lung fluid for our experiments was adapted from Gamble's solution [modified from Table 7 of Jurinski and Rimstidt (2001)], a solution that is considered similar to blood plasma [though with lower concentrations of albumin, globulin, fibronigen; Moss (1979); Kanapilly (1977); Mattson (1994)]. The difference between the simulated lung fluid used for aqueous experiments and that used for geochemical modeling is that for the aqueous experiments, we included organic acids with the major solution ions. Recall that thermodynamic data are not available for the all of the possible reactions of the included organic acids with the inorganic components of the minerals and fluid, and therefore organic acids were not included in the modeling. All other ion concentrations are the same for the aqueous experiments and the reaction-path modeling. The pH of the solution was adjusted to 7.4 using dilute  $\text{HNO}_3$ . The amount of nitric acid was minimal and we assume that little, if any, oxidation of the organic molecules occurred. The mixture of minerals used in these experiments originated from the Carey Canadian Deposit and was characterized by Gunter et al. (2007b). The mixture is mainly composed of brucite and chrysotile (Gunter et al. 2007b) and was chosen as representative of what a miner, miller, or other skilled trades-worker might be exposed to while working.

A 100 mL aliquot of Gamble's solution was added to 1 g of the mineral mixture. The reaction vessels were then placed in a shaker bath at 37 °C for six months. The mineral assemblage was then filtered and washed with DI water. Following a method developed by Sanchez and Gunter (2006) and Gunter et al. (2007b), the mineral assemblage was molded into a paste and, when dry, placed into a back-mount holder and analyzed using powder X-ray diffraction (XRD). Four-hour scans were performed on each sample with a Siemens D5000  $\theta$ - $\theta$  diffractometer equipped with a solid-state detector using  $\text{CuK}\alpha$  radiation, operating at 40 kV and 30 mA with a step size of 0.02 °2 $\theta$  from 5–40°. Count times were 9 s per step.

### Calcified pleural plaques

Calcified pleural plaques and surrounding tissue samples were acquired by the authors for scanning electron microscopy (SEM) and energy dispersive X-ray analysis (EDS). The pleural plaques were harvested from the autopsy of an 85 year old male who worked as a welder for 40 years and had a one-pack-a-day smoking habit as a young man. The plaques were critically point dried (a procedure used to prepare biological materials for SEM analysis that allows the biological material to retain structural integrity while under a vacuum) and imaged under a variable pressure scanning electron microscope at 15 to 18 kV. Backscattered electron imaging and elemental mapping were also performed to qualitatively determine mineral composition.

## RESULTS AND DISCUSSION

### Geochemical modeling: Dissolution rates

Dissolution rates, reflecting the residence time of a mineral in the lungs, as calculated in simulated lung fluid, from least to greatest, are: chrysotile < anorthite < K-feldspar < talc < muscovite = kaolinite = albite = quartz (none of the last four minerals dissolves appreciably over a 50 year time span). Figure 1 shows the calculated reaction progress in time for  $2 \times 2 \times 6 \mu\text{m}$  rectangular prisms of each mineral modeled (having a surface area of 10000  $\text{cm}^2/\text{g}$ ). When the mineral rate constants are taken into consideration, it is evident that these results are similar to the relative magnitudes of the mineral rate constants from greatest to least (Table 1). Surface area is additionally a critical controlling aspect of overall rates of mineral dissolution [Eqs. 1 and 2; Lasaga (1998)]; Figure 1 illustrates the difference between 10000  $\text{cm}^2/\text{g}$  ( $2 \times 2 \times 6 \mu\text{m}$ ) and 100000  $\text{cm}^2/\text{g}$  ( $0.2 \times 0.2 \times 0.6 \mu\text{m}$ ) chrysotile particles. Morphology is an important control on reaction rates as well and does affect mineral dissolution rates in lung fluids as pointed out by Jurinski and Rimstidt (2001) and Plumlee et al. (2006). Figure 1 also illustrates a difference in chrysotile dissolution rates in lung fluids as a function of morphology for occupational doses of spherical or rectangular prism shapes of chrysotile that is caused by both surface area and mass differences (because dose is measured as several particles per dry milligram of lung tissue).

Regardless of dose (occupational vs. environmental) or morphology (spheres vs. rectangular prisms), 99% of chrysotile particles with a 10000  $\text{cm}^2/\text{g}$  surface area dissolve within approximately one year and 99% of chrysotile particles with a 100000  $\text{cm}^2/\text{g}$  surface area dissolve in approximately one month (Fig. 1). Occupational exposures of 10000  $\text{cm}^2/\text{g}$  rectangular prisms (average size  $2 \times 2 \times 6 \mu\text{m}$ ) of quartz, kaolinite, muscovite, and albite do not appreciably dissolve over a 50 year span, while 99% of anorthite dissolves in five years, 99% of K-feldspar dissolves in 12 years, and 99% of talc dissolves in 35 years (Fig. 1). Hume and Rimstidt (1992) predicted that a chrysotile cylinder 1  $\mu\text{m}$  in diameter and infinitely long would take 9 ( $\pm 4.5$ ) months to

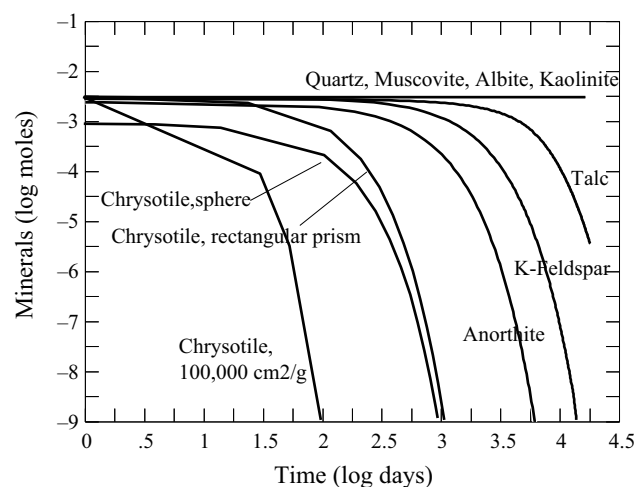


FIGURE 1. Consolidated predicted reaction-paths for mineral dissolution in simulated lung fluid at pH 7.4 from individual reaction-paths (see for example, Figs. 2–6).

dissolve using a shrinking fiber model. Parry (1985) predicted it would take six months for a  $1 \times 10 \mu\text{m}$  chrysotile fiber to dissolve by 30% based on calculated rates of  $\text{H}^+$  transport into cells and  $\text{Mg}^{2+}$  and  $\text{SiO}_2(\text{aq})$  out of cells. Jurinski and Rimstidt (2001) calculated the dissolution time of a  $1 \mu\text{m}$  sphere of chrysotile as seven months using a model similar to that of Hume and Rimstidt (1992). Wood et al. (2006) used reaction-path modeling to determine that, in a mixture with tremolite and chrysotile at pH 6.8, chrysotile dissolves after about 50 days.

Overall, our predicted dissolution times for chrysotile and talc are similar to earlier predictions (Hume and Rimstidt 1992; Parry 1985; Jurinski and Rimstidt 2001) as well as experimental data (Hume and Rimstidt 1992). Differences among the theoretical rates are largely related to the differences in modeling techniques. Hume and Rimstidt (1992) and Jurinski and Rimstidt (2001) use a shrinking sphere model to predict the lifetime of a particle in the lung. This equation is based on the particle diameter, the molar volume of particle, and the particle's rate constant. The shrinking sphere equation does not take into account fluid composition or saturation state as our modeling does, and saturation state affects the dissolution rate of a mineral. The GWB modeling framework calculates surface area at each step based on mineral mass and surface area per gram input values. Surface area does decrease with reaction progress similar to the shrinking core model but the function governing that surface area change is different.

The concentrations of muscovite, kaolinite, albite, and quartz remain relatively constant throughout the 50 year time period under physiologic conditions (Fig. 1). This is not surprising for two reasons. First, each of these minerals has a rate constant between  $10^{-16}$  and  $10^{-17}$  mol/cm<sup>2</sup>s, which means that they dissolve relatively slowly. Second, each of these phases is close to saturation in the model physiologic fluid. Therefore, because The Geochemist's Workbench calculates dissolution rates partly as a function of solution saturation state, one would predict that these minerals are kinetically inert under physiologic conditions.

#### Geochemical modeling: Secondary mineral formation in simulated lung fluids

The composition of the starting SLF (Table 4) is significantly supersaturated with respect to hydroxylapatite (Saturation Index,  $\text{SI} = \log Q/K$ , is 6.9). This is likely overestimated due to organic complexation of  $\text{Ca}^{2+}$  and P, but it is likely that the fluid is at least slightly oversaturated with respect to hydroxylapatite [discussed below, and as observed previously by Plumlee and Ziegler (2003)]. It is important to note that the aqueous composition of these lung fluids is not well constrained for some of the critical ions associated with mineralization, particularly associated with organic complexation. The goal of this geochemical modeling exercise is to investigate how primary minerals may dissolve in lung fluids and the types of secondary minerals they are likely to produce. We have done this in two ways surrounding the question of hydroxylapatite saturation states in lung fluids: (1) using an initial simulated lung fluid composition that was allowed to initially equilibrate with hydroxylapatite; and (2) using a simulated lung fluid composition that is supersaturated with respect to hydroxylapatite (Table 4). The results of the former will reflect any secondary mineralization directly related to primary mineral dissolution independent of existing supersaturation conditions.

The results of the latter will reflect precipitation of hydroxylapatite at each step in the flush model where each successive flush of fluid is supersaturated with respect to hydroxylapatite.

Results are presented in the figures discussed below in terms of log time (days) along the x-axis vs. amounts of primary minerals remaining and secondary minerals precipitating along the y-axis.

Chrysotile dissolution models in simulated lung fluids are presented using each combination of exposure (occupational and environmental), surface area (10 000 and 100 000 cm<sup>2</sup>/g), and morphology (spherical and rectangular prisms) in initially hydroxylapatite-supersaturated simulated lung fluids (Figs. 2a–2h). For chrysotile dissolution (Figs. 2a–2h), huntite [ $\text{CaMg}_3(\text{CO}_3)_4$ ] forms immediately and dissolves within approximately 2 to 500 days for each morphology, surface area, and dose. Talc also forms as the predominant reaction product of chrysotile dissolution



This suite of secondary precipitates differs from the minerals predicted to form as a result of chrysotile dissolution by Wood et al. (2006), however, those authors did not suppress dolomite. Talc dissolves in these models not as a function of dissolution kinetics, but as a function of undersaturated conditions prevailing as progressively smaller amounts of chrysotile dissolve [yielding lower amounts of Mg and  $\text{SiO}_2(\text{aq})$ ] as the particle mass and surface area decreases. In the 10 000 cm<sup>2</sup>/g surface area reactions (Figs. 2a–2d), talc is present under physiologic conditions from one month to 10 years depending on the chrysotile dose. In the 100 000 cm<sup>2</sup>/g surface area reactions (Fig. 2e–2h), talc dissolves within days (note that only primary mineral dissolution is kinetically constrained in these models. Dissolution of the secondary products is based solely on thermodynamics). However, when considering the slower dissolution rate of talc (models in which talc was the primary mineral indicate talc remains in the body for 2 to 35 years; Fig. 6), it is likely that, if talc does indeed form as a secondary product of chrysotile dissolution in the lung, it will not dissolve as quickly as over a period of days. Variations across all eight exposure scenarios for chrysotile (Figs. 2a–2h) illustrate the range of reaction differences possible as a result of varying mass and surface area; the secondary minerals and the processes governing their formation are identical, only the timing and amounts are different. Considering the dissolution of chrysotile in a fluid initially undersaturated with respect to hydroxylapatite (Figs. 2i and 2j), the mineralization is very similar with the exception of hydroxylapatite formation. It is noted, however, that precipitation of huntite at early stages of the model where the fluid is supersaturated with respect to hydroxylapatite inhibits hydroxylapatite formation (as huntite limits  $\text{Ca}^{2+}$  in solution) until the aqueous  $\text{Mg}^{2+}$  levels drop as a result of lower overall rates of chrysotile dissolution (due to less mass and, therefore, surface area).

The rate of fluid replenishment in lung tissue (the flushing rate) is a largely unconstrained variable, lacking more precise measurements in human lungs. To consider fluid replenishment, Figure 3 illustrates a different view of the modeling results from Figure 2c, namely looking at mineral changes as a function of  $\text{H}_2\text{O}$  reacted instead of time. Lower flushing rates

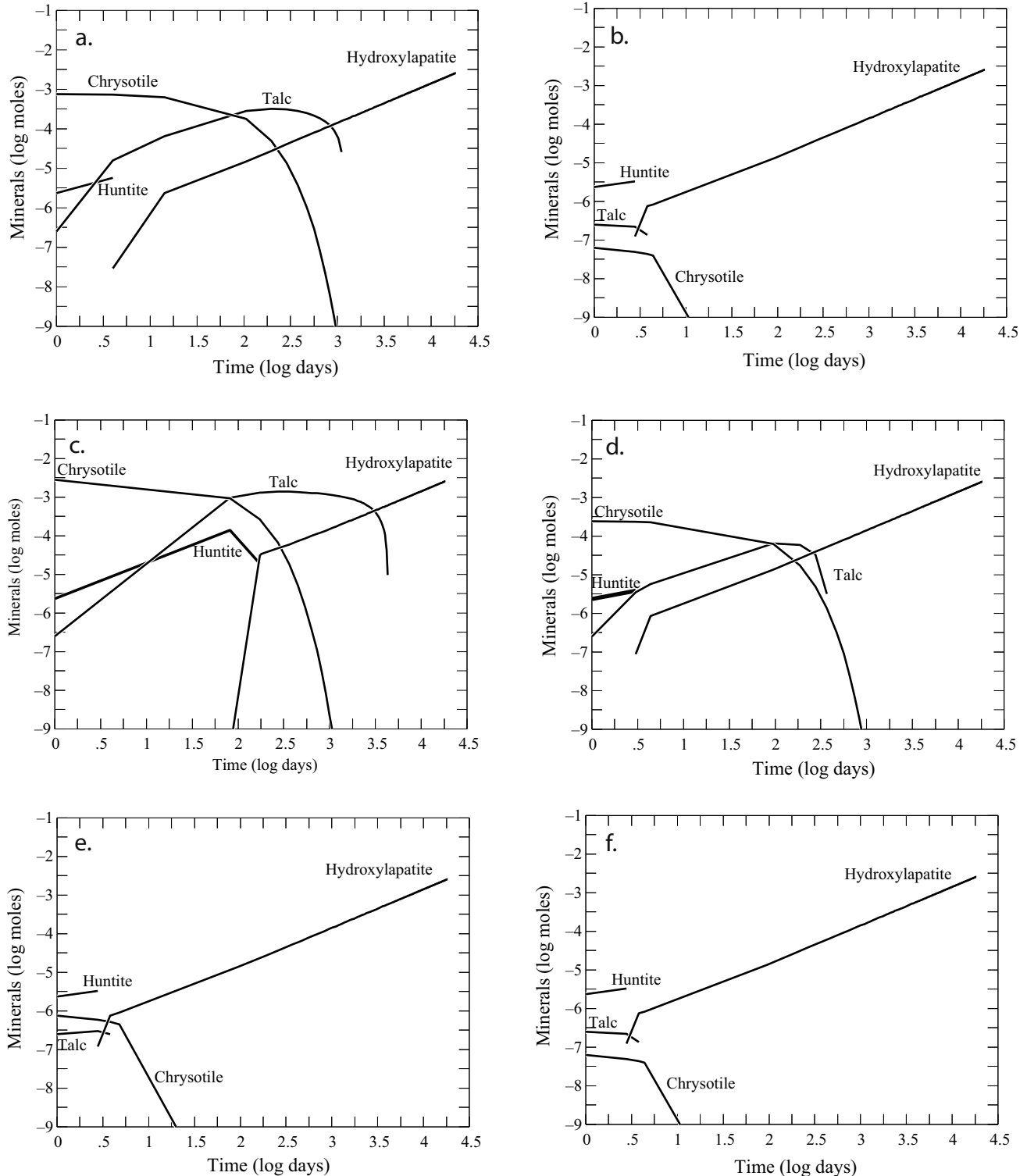


**FIGURE 2.** Complete reaction-paths for the simulated dissolution of chrysotile in simulated lung fluid at pH 7.4 with quartz, dolomite, and magnesite suppressed. Positive mineral slopes indicate predicted mineral precipitation. Negative slopes indicate predicted mineral dissolution. (a and b) Simulated dissolution of chrysotile spheres (s) with a total surface area of 10 000 cm<sup>2</sup>/g at environmental (25 000 particles/mg dry lung) and occupational (300 000 particles/mg dry lung) doses. (c and d) Simulated dissolution of chrysotile rectangular prisms (rp) with a total surface area of 10 000 cm<sup>2</sup>/g at environmental and occupational doses. (e and f) Simulated dissolution of chrysotile spheres (s) with a total surface area of 100 000 cm<sup>2</sup>/g at environmental and occupational doses. (Continued next page.)

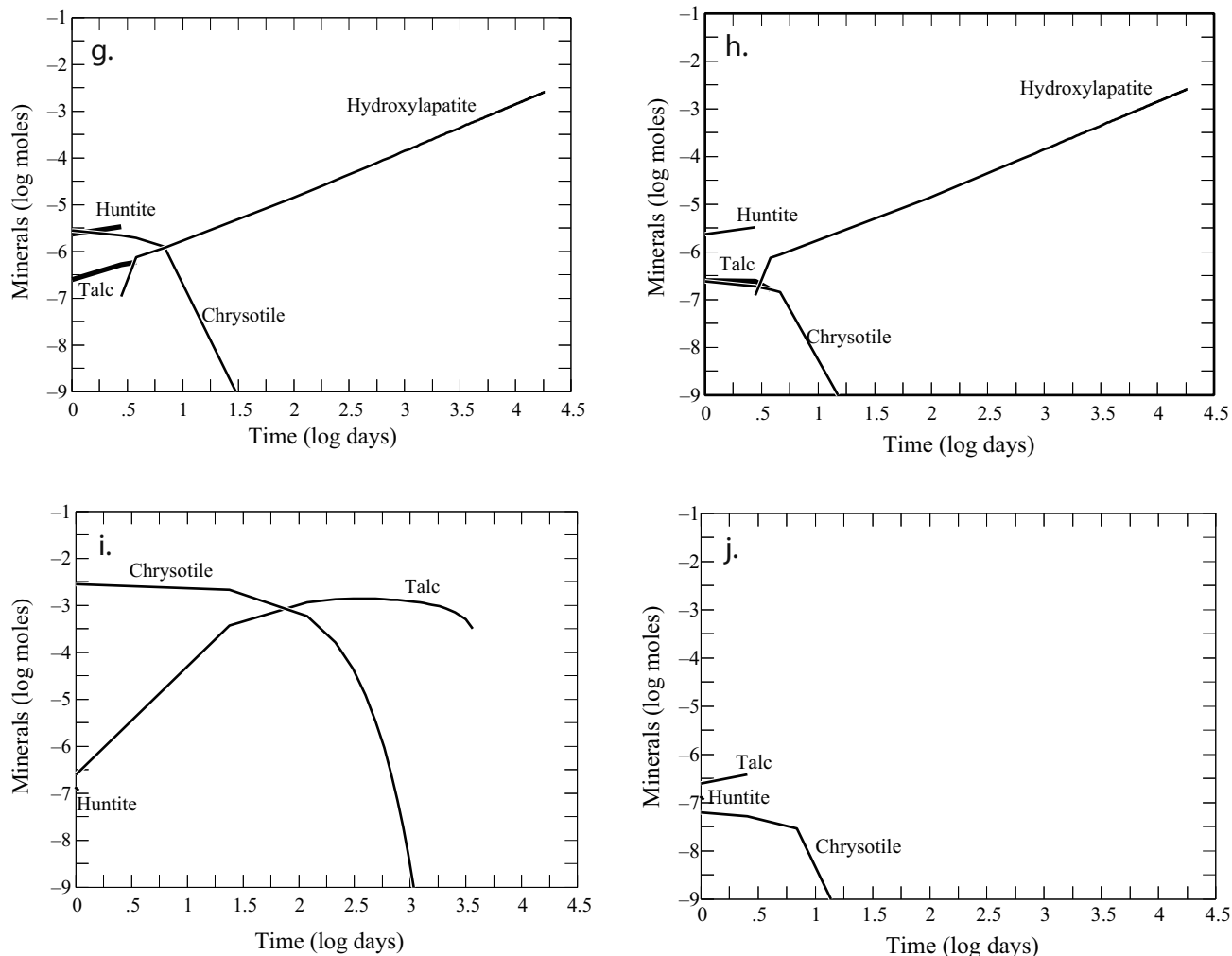
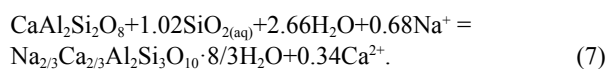


**FIGURE 2.—CONTINUED.** (g and h) Simulated dissolution of chrysotile rectangular prisms (rp) with a total surface area of 100 000 cm<sup>2</sup>/g at environmental and occupational doses. (i and j) Simulated dissolution of chrysotile rectangular prisms (rp) and spheres (s) at occupational and environmental doses (the two illustrated show the greatest range of dissolution) using a starting fluid and a flushing fluid that was undersaturated with respect to hydroxylapatite.

would result in it taking longer to react an equivalent amount of water through the system. Consistent with Figure 2c, huntite formation is constrained to initial conditions, in this case about 10 fluid replenishments over 10 days (100 g = 100 mL of fluid) are modeled to occur before hydroxylapatite and talc are the predominant secondary minerals to form and persist for extended periods of time.

Anorthite (CaAl<sub>2</sub>Si<sub>2</sub>O<sub>8</sub>) dissolution in lung fluids yields precipitation of diaspore [AlO(OH)] and mesolite (a zeolite: Na<sub>2/3</sub>Ca<sub>2/3</sub>Al<sub>2</sub>Si<sub>3</sub>O<sub>10</sub>·8/3H<sub>2</sub>O)



Figures 4a and 4b illustrates the range of timing and secondary mineral amounts possible for the extremes of dose and surface area (occupational dose of prisms at 10 000 cm<sup>2</sup>/g vs. environmental dose of spheres at 100 000 cm<sup>2</sup>/g). Mesolite was the most supersaturated zeolite calculated in the model and was

thus picked as to precipitate (other zeolite minerals were also supersaturated); a detailed experimental investigation of which zeolites may precipitate under these conditions might help constrain our models, but one does not exist to our knowledge.

K-feldspar dissolution (Fig. 5) is predicted to produce mesolite and celadonite [a clay mineral in the illite group, KMgAlSi<sub>4</sub>O<sub>10</sub>(OH)<sub>2</sub>]. For lower doses of K-feldspar, not enough dissolution occurs under model conditions to supersaturate these minerals and K-feldspar is predicted to dissolve without formation of any secondary minerals (recall hydroxylapatite formation results from an already supersaturated fluid composition).

Huntite is the only secondary mineral, other than hydroxylapatite, predicted to precipitate during talc dissolution (Fig. 6). Jurinski and Rimstidt (2001) did not analyze the reacted solids in their dissolution experiment, but our model results suggest that, in physiological fluids under the flushing rates established, secondary minerals would not form. We note, however, that lower flushing rates may cause more significant supersaturation of secondary minerals.

Mesolite is predicted to precipitate in some of the reactions involving muscovite, kaolinite, and albite [not illustrated; see

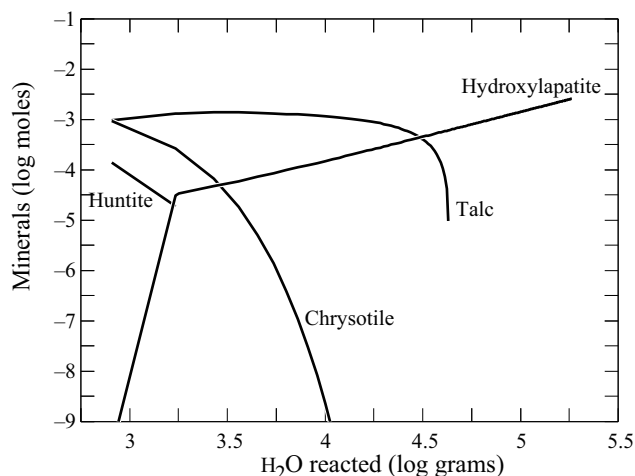


**FIGURE 3.** Simulated dissolution of chrysotile rectangular prisms (rp) with a total surface area of 10 000 cm<sup>2</sup>/g at occupational dosing plotted with the amount of H<sub>2</sub>O flushed along the x-axis. Note that this simulates how variations in flushing rate (i.e., the amount of H<sub>2</sub>O that has contacted the chrysotile in time) affect secondary mineral assemblages.

Taunton (2007)], but because the rate of reaction is very slow (Fig. 1), very high doses of these minerals would be required to cause supersaturation of zeolite minerals such as mesolite. Even at higher doses, calcite and quartz dissolution reactions produce no secondary phases other than hydroxylapatite (calcite dissolution would increase the amount of hydroxylapatite forming due to an increase in Ca<sup>2+</sup> ion dissolution into the fluid).

Crystalline or amorphous silica phases have often been observed as a product of primary mineral dissolution, including the dissolution of chrysotile (Favero-Longo et al. 2005) and talc (Jurinski and Rimstidt 2001). Our modeling suppressed formation of quartz, as quartz would not be the first silica phase to precipitate under these conditions (Icopini et al. 2005). All other forms of silica (e.g., opal, cristobalite, tridymite) remained undersaturated in our theoretical system as silica was taken up by a silicate phase such as talc, mesolite, or celadonite before a non-quartz silica phase became supersaturated. Incongruent dissolution of primary phases such as chrysotile or feldspars may release silica at a slower rate than other ions (Jurinski and Rimstidt 2001; Hellman et al. 2003; Icopini et al. 2005; Wood et al. 2006), which may change how, and if, some secondary phases form.

Several of the primary minerals discussed here are associated with respiratory disease: talc, quartz, kaolinite (Ross et al. 1993), and chrysotile and tremolite (e.g., Churg 2001). Out of all of the secondary minerals predicted to precipitate, only talc is suggested to cause respiratory disease (Ross et al. 1993). However, what is unknown about these predicted secondary phases is their crystallinity (i.e., the morphology and size), which is an important unresolved issue, specifically concerning the physical and/or geochemical interactions with cells, and the effect on disease processes.

As stated earlier, chrysotile, talc, kaolinite, and quartz have all been implicated in respiratory disease. Why do we not see respiratory disease associated with feldspar or muscovite exposure?

According to reaction-path modeling, these minerals are just as biodurable (and even more so than chrysotile) as pathologic minerals. One reason might be that mechanical factors could be at play. Plumlee et al. (2006) notes that minerals be inhaled deep into the lungs in order to cause disease. Larger particles (tens of micrometers, possibly the diameter of sheet silicates) are deposited in the upper airways and cleared by mechanical means such as increased mucus production and coughing. Smaller particles (<2 μm) can travel to the alveoli, the air sacs of the lungs, and become lodged there. In this environment, particles must be dissolved by chemical or cellular means [i.e., phagocytosis, see Plumlee et al. (2006)].

It is interesting to note the predicted formation of aluminous phases such as diaspore, mesolite, and celadonite under physiological conditions. Diaspore is not as common as other Al-oxide

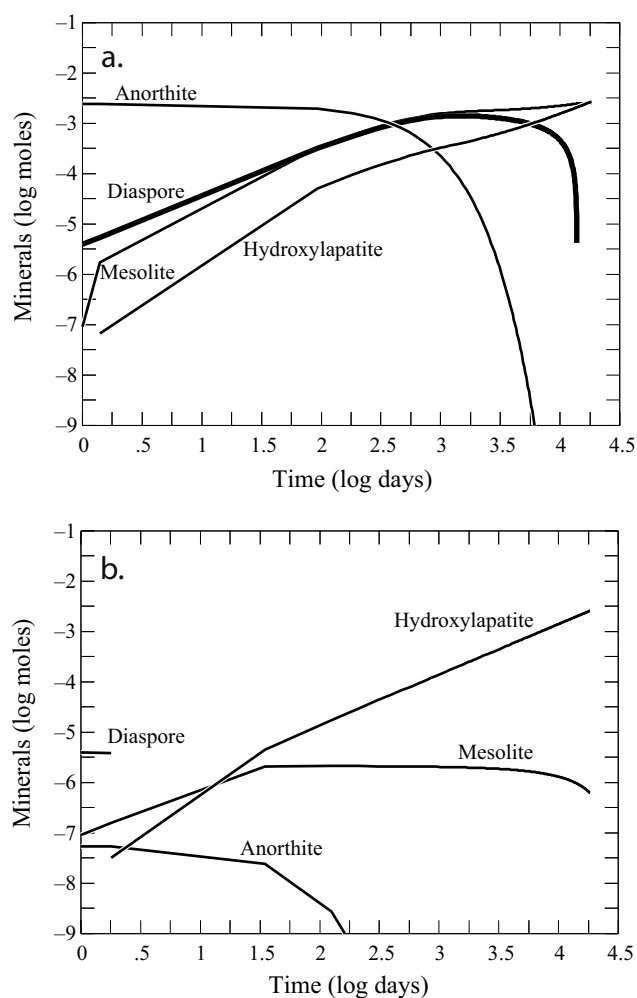


**FIGURE 4.** Reaction-paths for the simulated dissolution of anorthite in simulated lung fluid at pH 7.4 with quartz, dolomite, and magnesite suppressed. Positive mineral slopes indicate predicted mineral precipitation. Negative slopes indicate predicted mineral dissolution. (a) Simulated dissolution of anorthite rectangular prisms (rp) with a total surface area of 10 000 cm<sup>2</sup>/g at an occupational (300 000 particles/mg dry lung) dose. (b) Simulated dissolution of anorthite spheres (s) with a total surface area of 100 000 cm<sup>2</sup>/g at an environmental (25 000 particles/mg dry lung) dose.

or Al-hydroxide minerals formed in nature such as gibbsite and boehmite (Sparks 1995). However, it is known to precipitate at low temperatures (Amram and Ganor 2004). Mesolite occurs in basalts and hydrothermal systems and is also found as weathering products in low-temperature systems. Likewise, celadonite is an aqueous weathering product in the environment. Given the uncertainty inherent in the modeling construct and in the thermodynamic data for mineral phases, these specific phases may not be what would be observed in the lung, but suggest that some mixture of aluminum/aluminosilicate phases are important in controlling aluminum mobility in the lungs. In reference to physiologic conditions, elevated aluminum concentrations are most notably associated with Alzheimer's disease (Perl and Moalem 2006). In fact, Candy et al. (1986) reported that senile lesions that, in part, define Alzheimer's disease, contained dense

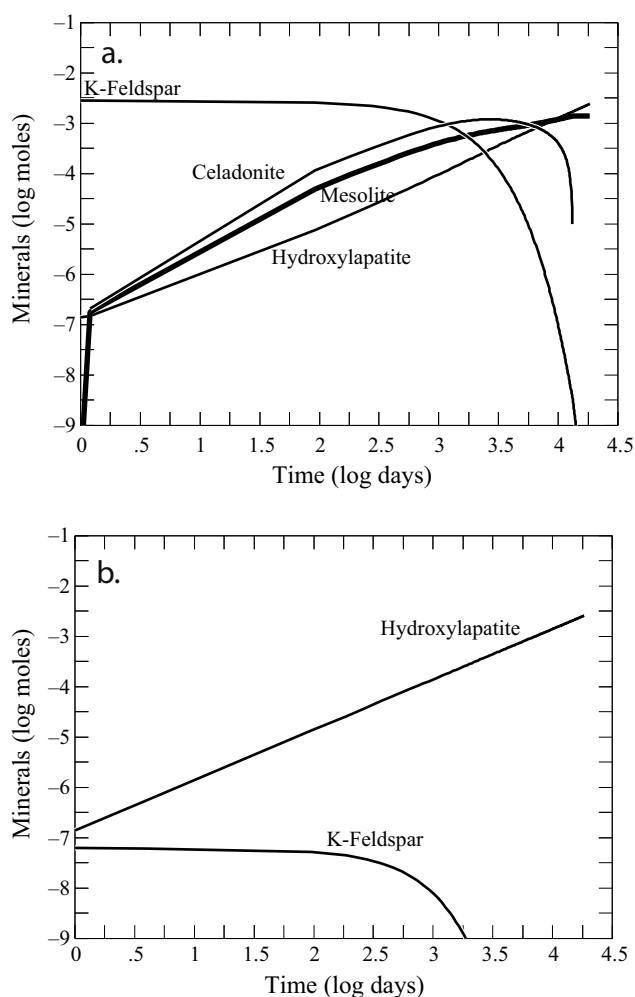


**FIGURE 5.** Complete reaction-paths for the simulated dissolution of K-feldspar in simulated lung fluid at pH 7.4 with quartz, dolomite, and magnesite suppressed. Positive mineral slopes indicate predicted mineral precipitation. Negative slopes indicate predicted mineral dissolution. (a) Simulated dissolution of K-feldspar rectangular prisms (rp) with a total surface area of 10 000 cm<sup>2</sup>/g at an occupational (300 000 particles/mg dry lung) dose. (b) Simulated dissolution of K-feldspar rectangular prisms (rp) with a total surface area of 100 000 cm<sup>2</sup>/g at an occupational (300 000 particles/mg dry lung) dose.

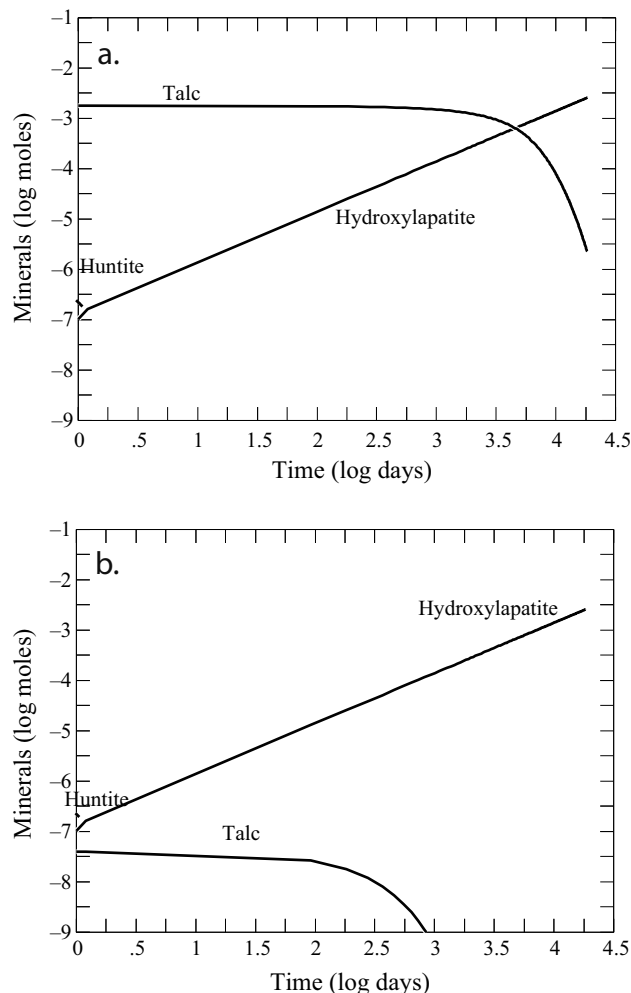


**FIGURE 6.** Complete reaction-paths for the simulated dissolution of talc in simulated lung fluid at pH 7.4 with quartz, dolomite, and magnesite suppressed. Positive mineral slopes indicate predicted mineral precipitation. Negative slopes indicate predicted mineral dissolution. (a) Simulated dissolution of talc rectangular prisms (rp) with a total surface area of 10 000 cm<sup>2</sup>/g at an occupational (300 000 particles/mg dry lung) dose. (b) Simulated dissolution of talc spheres (s) with a total surface area of 100 000 cm<sup>2</sup>/g at an environmental (25 000 particles/mg dry lung) dose.

aluminosilicate cores. Our modeling results illustrate the possible formation of aluminum-bearing minerals in the body that warrants greater attention when considering the health effects of minerals.

#### Aqueous experiments

X-ray diffraction analysis of the brucite/chrysotile mineral assemblage after six months in a batch reactor, with a simulated lung fluid, shows that brucite and chrysotile are still present (Fig. 7). Additionally, hydroxylapatite formed. The ratio of the brucite peak to the chrysotile peak is lower in the reacted material than in the unreacted material. This indicates that brucite dissolves more quickly than chrysotile. This is not surprising because the dissolution rate constant for brucite is six orders of magnitude higher than that of chrysotile (Nagy 1995). A flush model for

these multiple minerals proved impossible with our modeling efforts, but brucite and chrysotile mineral dissolution can easily be modeled using The Geochemist's Workbench without the flush option (a model more appropriate when comparing experimental results). Results from modeling under these experimental are presented in Figure 8. Kinetic data for brucite were estimated after the Nagy (1995) observations (indicating that brucite dissolves six orders of magnitude faster than chrysotile), though modeling presented is conservatively estimated as a four-order-of-magnitude difference. Note that brucite is expected to react almost completely after about two weeks with a model that likely underestimates the actual reaction rate, yet experimental evidence (Fig. 7) indicates significant brucite remains after six months. The model assumes, however, that the particle surfaces remain accessible; precipitation of secondary minerals on mineral surfaces or sorption of ions onto those surfaces can inhibit dissolution (for review see Brezonik 1994; Brantley et al. 2008). Also of note is that the model predicts the formation of hydromagnesite; brucite dissolution is known to form this mineral (Xiong 2007; Xiong and Lord 2008), yet the XRD pattern does not indicate any peaks for hydromagnesite. One possibility to describe the lack of hydromagnesite peaks is the formation of nanocrystalline hydromagnesite that would be X-ray amorphous, or through inhibition (or "armoring") of primary minerals with hydroxylapatite that limited hydromagnesite precipitation to an amount that was below XRD detection limits.

### Calcified pleural plaques

Calcified pleural plaques are considered as biomarkers for asbestos exposure but not for quartz exposure. Variable-pressure

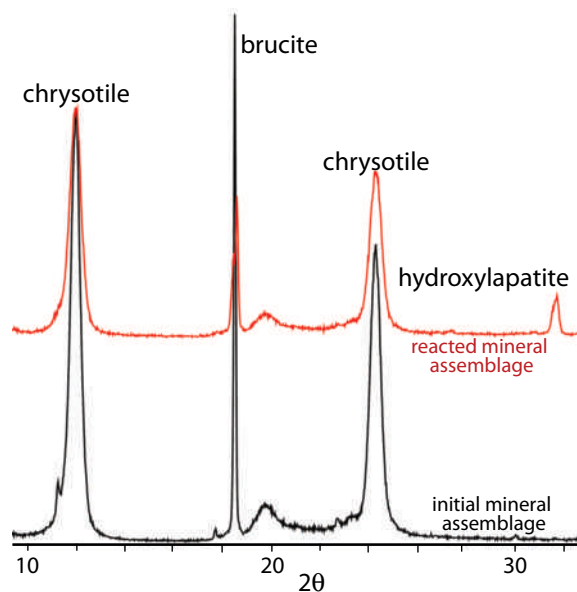


**FIGURE 7.** Powder X-ray diffraction pattern of unreacted (bottom scan) and reacted (top scan) mineral assemblage in batch reactions of brucite and chrysotile in simulated lung fluid at pH 7.4. The unreacted mineral assemblage is the brucite/chrysotile starting material. The reacted mineral assemblage is the initial mineral assemblage after six months in the batch reactor under simulated physiologic conditions. Note the decrease in the amount of brucite present and the presence of hydroxylapatite in the reacted mineral assemblage.

scanning electron microscopy of calcified pleural plaques and associated tissues reveals the presence of various minerals (mostly calcium phosphates). Figure 9 depicts an occurrence of one such calcium phosphate mineral in both secondary electron and backscattered electron images. The mineral grain is roughly 30  $\mu\text{m}$  in length and 10  $\mu\text{m}$  in width. Elemental mapping and energy dispersive X-ray analysis both confirm that it is a calcium-phosphate "mineral" (Taunton 2007). The dimensions of this particular mineral grain are of interest for this project. Inhalation of particles occurs daily in humans. However, for a particle to travel all the way to the lungs, certain morphological criteria have to be met. Namely, the dimensions of the particle must be less than about 2  $\mu\text{m}$  in diameter to reach the deepest parts of the lung (Plumlee et al. 2006) where this plaque occurred. Thus, the large dimensions of this particle necessitate that it precipitated in place, again supporting the reaction-path modeling results and the likelihood that lung fluids are indeed supersaturated with respect to hydroxylapatite. Whereas the formation of calcium phosphate crystals as bones and teeth in the body is a complicated, well-studied process involving highly specialized "bone-making" cells (Glimcher 2006), the processes by which calcium phosphate crystals not associated with bones or teeth form in the body is unclear. From the batch experiments and reaction-path modeling discussed, hydroxylapatite can precipitate under simulated lung conditions without any programmed assistance from cells. However, one must assume that, because hydroxylapatite is not found everywhere in the body, there must be other controls involved in the precipitation of this mineral. For example, perhaps cells contribute to the complexation of calcium by producing organic molecules, keeping hydroxylapatite from being saturated. McCance and Huether (2002) described the process of tissue calcification as involving an influx of extracellular calcium into damaged mitochondria. A process that is specific to alveoli in the lungs involves acid excretion around the alveoli that locally creates an internal increase but an external decrease

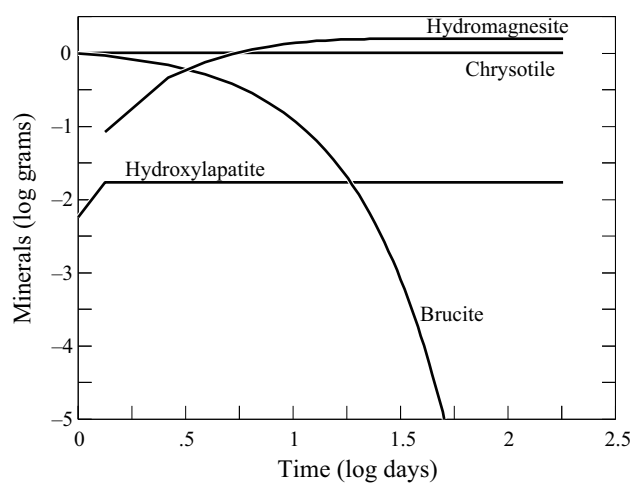


**FIGURE 8.** Complete reaction-paths for the simulated dissolution of mixture of brucite and chrysotile in simulated lung fluid at pH 7.4 with quartz, dolomite, and magnesite suppressed. Positive mineral slopes indicate predicted mineral precipitation. Negative slopes indicate predicted mineral dissolution. This is a titration simulation, not a flush model, consistent with the experimental setup.

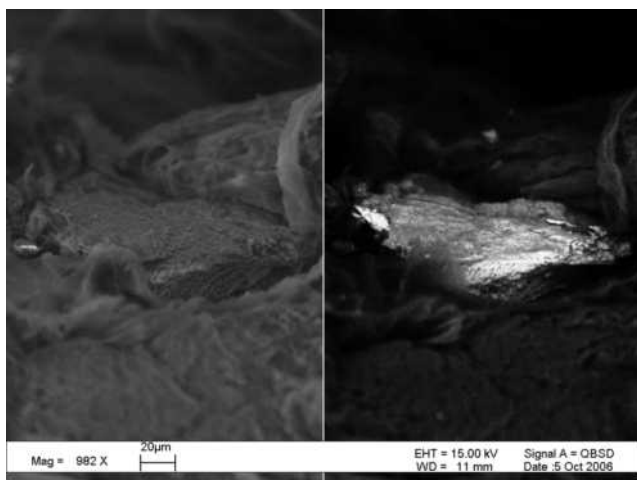
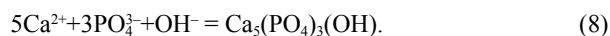


**FIGURE 9.** Variable pressure scanning electron image (left) and backscattered electron image (right) of a calcium-phosphate particle in the lung.

in hydroxyl ions; pH change drives dissolution/precipitation of hydroxyapatite, affecting the concentration of  $\text{OH}^-$ :



Additionally, organic ligands are known to affect silicate dissolution rates (Cama and Ganor 2006; Golubev and Pokrovsky 2006; Welch and Ullman 2000; Blum and Stillings 1995), and can enhance dissolution of apatite thermodynamically by complexing  $\text{Ca}^{2+}$  with an organic acid (decreasing  $\text{Ca}^{2+}$  in Eq. 8 and driving the reaction to the left).

### CONCLUDING REMARKS

Reaction-path modeling of rock-forming minerals under physiologic conditions (Figs. 1–6, 8) is a unique approach to combining geochemistry, mineralogy, and medical science. Our results represent some of the first to provide geochemical insight into the behavior of minerals under simulated lung fluid conditions and the possible formation of secondary minerals. Reaction rates, available surface area, stability of minerals in lung fluid, fluid replenishment rates, and mineral dose are critical factors to assess mineral durability and secondary mineral formation in human lung tissue. The model prediction of the secondary mineralization of talc, hydroxylapatite, huntite, diaspore, mesolite, and celadonite may additionally be a key factor in considering biodurability and physiological reactions in lung tissue. The prediction that the dissolution of Al-bearing minerals leads to the precipitation of aluminum/aluminosilicate minerals such as diaspore, mesolite, and celadonite is interesting in light of the association of  $\text{Al}^{3+}$  and aluminosilicates with Alzheimer's disease. These results should be considered when addressing pathways of aluminum in the human body. Results from batch experiments and modeling confirm the formation of calcium phosphate minerals, namely hydroxylapatite, under simulated lung fluid conditions. Variable-pressure SEM analysis of lung tissue also confirms the precipitation of calcium-phosphate minerals in the lung independent of teeth and bone formation (Taunton 2007).

We hope to highlight that there are significant limitations in the current state of knowledge surrounding the aqueous composition of lung fluids, physiological fluid replenishment rates, and secondary mineral crystallinity; all of these factors likely have significant implications for how mineral inhalation affects human health. Additionally, these models and other attempts to understand the reactivity of minerals in lung fluids would benefit greatly from mineral-fluid reaction studies including detailed mineralogical analysis and the determination of rate constants in more appropriate solutions; such information would help to constrain modeling approaches. All of these results demonstrate that geochemical tools can provide important insights to the medical community; collaboration between geologists and medical professionals can only help continue to refine the understanding of specific mineral reactions in humans and the possible health effects.

### ACKNOWLEDGMENTS

We thank Don Rimstidt, Geoff Plumlee, and Martin Schoonen for their many suggestions that helped improve this manuscript.

### REFERENCES CITED

- Aage, H.K., Andersem B.L., Blom, A., and Jensen, I. (1997) The solubility of struvite. *Journal of Radioanalytical and Nuclear Chemistry*, 223, 213–215.
- Amram, K. and Ganor, J. (2004) The combined effect of pH and temperature on smectite dissolution rate under acidic conditions. *Geochimica et Cosmochimica Acta*, 69, 2535–2546.
- Bethke, C.M. (1996) *Chemical Reaction Modeling*. Oxford University Press, New York.
- Bhuiyan, M.I.H., Mavinic, D.S., and Beckie, R.D. (2007) A solubility and thermodynamic study of struvite. *Environmental Technology*, 28, 1015–1026.
- Blum, A.E. and Stillings, L.L. (1995) Feldspar dissolution kinetics. In A.F. White and S.L. Brantley, Eds., *Chemical Weathering Rates of Silicate Minerals*, 31, p. 291–351. Reviews in Mineralogy, Mineralogical Society of America, Chantilly, Virginia.
- Borda, M.J., Elsetinow, A.E., Strongin, D.R., and Schoonen, M.A.A. (2003) A mechanism for the production of hydroxyl radical at surface defect sites on pyrite. *Geochimica et Cosmochimica Acta*, 67, 935–939.
- Brantley, S.L., Kubicki, J.D., and White, A.F. (2008) *Kinetics of Water-rock Interaction*, 196 p. Springer, New York.
- Brezonik, P.L. (1993) *Chemical Kinetics and Process Dynamics in Aquatic Systems*, 754 p. CRC Press, Ann Arbor, Michigan.
- Cama, J. and Ganor, J. (2006) The effects of organic acids on the dissolution of silicate minerals: A case study of oxalate catalysis of kaolinite dissolution. *Geochimica et Cosmochimica Acta*, 70, 2191–2209.
- Candy, J.M., Oakley, A.E., Klinowski, J., Carpenter, T.A., Perry, R.H., Atach, J.R., Perry, E.K., Blessed, G., Fairbairn, A., and Edwardson, J.A. (1986) Aluminosilicates and senile plaque formation in Alzheimer's disease. *Lancet*, 1, 354–357.
- Carroll, S.A. and Walther, J.V. (1990) Kaolinite dissolution at 25 °C, 60 °C, and 80 °C. *American Journal of Science*, 290, 797–810.
- Chou, L., Garrels, R.M., and Wallast, R. (1989) Comparative study of the kinetics and mechanisms of dissolution of carbonate minerals. *Chemical Geology*, 78, 269–282.
- Churg, A. (2001) Pathological findings in the lungs of long-term Quebec chrysotile miners and millers: An analysis of 247 cases. In R.P. Nolan, A.M. Langer, M. Ross, F.J. Wicks, and R.F. Martin, Eds., *The Health Effects of Chrysotile Asbestos: Contribution of science to risk-management decisions*, p. 207–211. Mineralogical Association of Canada, Ontario.
- Cohn, C.A., Laffers, R., Simon, S.R., O'Riordan, T., and Schoonen, M.A.A. (2006) Role of pyrite in formation of hydroxyl radicals in coal: Possible implications for human health. *Particle and Fibre Toxicology*, 3, 1–10.
- Davis, J.M.G. (2001) In vivo assays to evaluate the pathogenic effects of minerals in rodents. In R.P. Nolan, A.M. Langer, M. Ross, F.J. Wicks, and R.F. Martin, Eds., *The Health Effects of Chrysotile Asbestos: Contribution of science to risk-management decisions*, p. 471–487. Mineralogical Association of Canada, Ontario.
- Drever, J.I. (1994) The effects of land plants on weathering rates of silicate minerals. *Geochimica et Cosmochimica Acta*, 58, 2325–2332.
- Dutta, D. and Moudgil, B.M. (2007) Crystalline silica particles mediated lung injury. *Kona-Powder and Particle*, 25, 76–87.
- Favero-Longo, S., Turci, F., Tomatis, M., Castelli, D., Bonfante, P., Hochella, M.F.,

- Piervittori, R., and Fubini, B. (2005) Chrysotile asbestos is progressively converted into a non-fibrous amorphous material by the chelating action of lichen metabolites. *Journal of Environmental Monitoring*, 7, 764–766.
- Forde, S., Hynes, M.J., and Jonson, B. (2008) Dissolution of glass compositions containing no lead in simulated lung fluid. *International Journal of Hygiene and Environmental Health*, 211, 357–366.
- Gault, M.H., Chafe, L., Longerich, L., and Mason, R.A. (1993) Calcium and calcium magnesium carbonate specimens submitted as urinary tract stones. *Journal of Urology*, 149, 244–249.
- Glimcher, M.J. (2006) Bone: Nature of the calcium phosphate crystals and cellular, structural, and physical chemical mechanisms in their formation. In N. Sahai and M.A.A. Schoonen, Eds., *Medical Mineralogy and Geochemistry*, 64, p. 223–282. Reviews in Mineralogy and Geochemistry, Mineralogical Society of America, Chantilly, Virginia.
- Golubev, S.V. and Pokrovsky, O.S. (2006) Experimental study of the effect of organic ligands on diopside dissolution kinetics. *Chemical Geology*, 235, 377–389.
- Govindaraju, K., Cowley, E.A., Eidelman, D.H., and Lloyd, D.K. (1997) Microanalysis of lung airway surface fluid by capillary electrophoresis with conductivity detection. *Analytical Chemistry*, 69, 2793–2797.
- Gunter, M.E. (1999) Quartz—The most abundant mineral species in the earth's crust and a human carcinogen? *Journal of Geoscience Education*, 47, 341–349.
- Gunter, M.E., Belluso, E., and Mottana, A. (2007a) Amphiboles: Environmental and health concerns. In F.C. Hawthorne, R. Oberti, G. Della Ventura, and A. Mottana, Eds., *Amphiboles: Crystal chemistry, occurrences, and health concerns*, 67, p. 453–516. Reviews in Mineralogy and Geochemistry, Mineralogical Society of America, Chantilly, Virginia.
- Gunter, M.E., Sanchez, M.S., and Williams, T.J. (2007b) Characterization of chrysotile samples for the presence of amphiboles from the Carey Canadian deposit, southeastern Quebec, Canada. *Canadian Mineralogist*, 45, 263–280.
- Guthrie, G.D. and Mossman, B.T., Eds. (1993) *Health Effects of Mineral Dusts*, vol. 28. Mineralogical Society of America, Chantilly, Virginia.
- Hellman, R. (1994) The albite-water system: Part I. The kinetics of dissolution as a function of pH at 100, 200, and 300 °C. *Geochimica et Cosmochimica Acta*, 58, 595–611.
- Hellman, R., Penisson, J.M., Hervig, R.L., Thomassin, J.H., and Abrioux, M.F. (2003) An EFTEM/HRTEM high-resolution study of the near surface of labradorite feldspar altered at acid pH: Evidence for interfacial dissolution-reprecipitation. *Physics and Chemistry of Minerals*, 30, 192–197.
- Hewitt, C.D., Winbome, K., Margrey, O., Nicholson, J.R.P., Savory, M.G., Savory, J., and Wills, M.A. (1990) Critical appraisal of two methods of determining aluminum in blood samples. *Clinical Chemistry*, 36, 1466–1469.
- Hume, L.A. and Rimstidt, J.D. (1992) The biodegradability of chrysotile asbestos. *American Mineralogist*, 77, 1125–1128.
- Icopini, G.A., Brantley, S.L., and Heaney, P.J. (2005) Kinetics of silica oligomerization and nanocolloid formation as a function of pH and ionic strength at 25 °C. *Geochimica et Cosmochimica Acta*, 69, 293–303.
- Jurinski, J.B. and Rimstidt, J.D. (2001) Biodegradability of talc. *American Mineralogist*, 86, 392–399.
- Kanapilly, G.M. (1977) Alveolar microenvironment and its relationship to the retention and transport into blood or aerosols deposited in the alveoli. *Health Physics*, 32, 89–100.
- Knauss, K.G., Nguyen, S.N., and Weed, H.C. (1993) Diopside dissolution kinetics as a function of pH, CO<sub>2</sub>, temperature, and time. *Geochimica et Cosmochimica Acta*, 57, 285–294.
- Kofina, A.N. and Koutsoukos, P.G. (2005) Spontaneous precipitation of struvite from synthetic wastewater solutions. *Crystal Growth and Design*, 5, 489–496.
- Langmuir, D. (1997) *Aqueous Environmental Chemistry*. Prentice Hall, New Jersey.
- Lasaga, A.C. (1998) *Kinetic Theory in Earth Sciences*. Princeton University Press, New Jersey.
- Lasaga, A.C., Soler, J.M., Ganor, J., Burch, T.E., and Nagy, K.L. (1994) Chemical weathering rate laws and global geochemical cycles. *Geochimica et Cosmochimica Acta*, 58, 2361–2386.
- Mansfield, C.F. (1980) A urolith of biogenic dolomite—Another clue in the dolomite mystery. *Geochimica et Cosmochimica Acta*, 44, 829–831.
- Mattson, S.M. (1994) Glass fiber dissolution in simulated lung fluid and measures needed to improve consistency and correspondence to in vivo dissolution. *Environmental Health Perspectives*, 102, 87–90.
- McCance, K.L. and Huether, S.E. (2002) *Pathophysiology: The biologic basis for disease in adults and children*. Mosby, Inc., Missouri.
- McDonald, J.C. and McDonald, A.C. (1997) Chrysotile, tremolite and carcinogenicity. *Annals of Occupational Hygiene*, 41, 699–705.
- Moss, O.R. (1979) Simulants of interstitial fluid. *Health Physics*, 36, 447–448.
- Nagy, K.L. (1995) Dissolution and precipitation kinetics of sheet silicates. In A.F. White and S.L. Brantley, Eds., *Chemical Weathering Rates of Silicate Minerals*, 31, p. 173–233. Reviews in Mineralogy, Mineralogical Society of America, Chantilly, Virginia.
- Norton, M.R. and Gunter, M.E. (1999) Relationships between respiratory diseases and quartz-rich dust in Idaho. *American Mineralogist*, 84, 1009–1019.
- Osborne, C.A., Oldroyd, N.O., and Clinton, C.W. (1986) Etiopathogenesis of uncommon canine uroliths. Xanthine, carbonate, drugs, and drug metabolites. *Veterinary Clinic of North America Small Animal Practice*, 16, 217–225.
- Paces, T. (1983) Rate constants of dissolution derived from the measurements of mass balance in hydrological catchments. *Geochimica et Cosmochimica Acta*, 47, 1855–1863.
- Pagana, K.D. and Pagana, T.J. (2001) *Mosby's diagnostic and laboratory test reference*, 984 p. Harcourt Health Sciences, St. Louis.
- Parry, W.T. (1985) Calculated solubility of chrysotile asbestos in physiological systems. *Environmental Research*, 37, 410–418.
- Perl, D.P. and Moalem, S. (2006) Aluminum, Alzheimer's Disease and the geospatial occurrence of similar disorders. In N. Sahai and M.A.A. Schoonen, Eds., *Medical Mineralogy and Geochemistry*, 64, p. 115–134. Reviews in Mineralogy and Geochemistry, Mineralogical Society of America, Chantilly, Virginia.
- Plumlee, G.S., Morman, S.A., and Ziegler, T.L. (2006) The toxicological geochemistry of earth materials: An overview of processes and the interdisciplinary methods used to understand them. In N. Sahai and M.A.A. Schoonen, Eds., *Medical Mineralogy and Geochemistry*, 64, p. 5–57. Reviews in Mineralogy and Geochemistry, Mineralogical Society of America, Chantilly, Virginia.
- Plumlee, G.S. and Ziegler, T.L. (2003) The medical geochemistry of dusts, soils, and other earth materials. In B.S. Loller, Ed., *Environmental Geochemistry*, 9, p. 263–310. Treatise on Geochemistry, Elsevier, Amsterdam.
- Ross, M., Nolan, R.P., Langer, A.M., and Cooper, W.C. (1993) Health effects of mineral dusts other than asbestos. In G.D. Guthrie and B.T. Mossman, *Health Effects of Mineral Dusts*, 28, p. 361–407. Reviews in Mineralogy, Mineralogical Society of America, Chantilly, Virginia.
- Sanchez, M.S. and Gunter, M.E. (2006) Quantification of amphibole content in expanded vermiculite products from Libby, Montana U.S.A. *American Mineralogist*, 91, 1448–1501.
- Skinner, H.C.W. (2005) *Mineralogy of bone*. In O. Selinus, B. Alloway, J.A. Centeno, R.B. Finkelman, R. Fuge, U. Lindh, and P. Smedley, *Essentials of Medical Geology: Impacts of the natural environment on public health*, p. 667–693. Elsevier, Amsterdam.
- Sparks, D.L. (1995) *Environmental Soil Chemistry*. Academic Press, California.
- Sutton, M. and Burastero, S.R. (2003) Beryllium chemical speciation in elemental human biological fluids. *Chemical Research in Toxicology*, 16, 1145–1154.
- Sutton, M. and Burastero, S.R. (2004) Uranium(VI) solubility and speciation in simulated elemental human biological fluids. *Chemical Research in Toxicology*, 17, 1468–1480.
- Takaya, M., Shinohara, Y., Serita, F., Ono-Ogasawara, M., Otaki, N., Toya, T., Takata, A., Yoshida, K., and Kohyama, N. (2006) Dissolution of functional materials and rare earth oxides into pseudo alveolar fluid. *Industrial Health*, 44, 639–644.
- Taunton, A.E. (2007) *Mineralogy and geochemistry in the lung*, 129 p. Ph.D. dissertation, University of Idaho, Moscow, Idaho.
- Van Oss, C.J., Naim, J.O., Constanzo, P.M., Giese, R.F., Wu, W., and Sorling, A.F. (1999) Impact of different asbestos species and other mineral particles on pulmonary pathogenesis. *Clays and Clay Minerals*, 47, 697–707.
- Welch, S.A. and Ullman, W.J. (2000) The temperature dependence of bytownite feldspar dissolution in neutral aqueous solutions of inorganic and organic ligands at low temperature 5–35 °C. *Chemical Geology*, 167, 337–354.
- Wood, S.A., Taunton, A.E., Normand, C., and Gunter, M.E. (2006) Mineral-fluid interactions in the lungs: Insights from reaction path modeling. *Inhalation Toxicology*, 18, 975–984.
- Xiong, Y. (2008) Thermodynamic properties of brucite determined by solubilization studies and their significance to nuclear waste isolation. *Aquatic Geochemistry*, 14, 223–238.
- Xiong, Y. and Lord, A.C.S. (2008) Experimental investigations of the reaction path in the MgO-CO<sub>2</sub>-H<sub>2</sub>O system in solutions with various ionic strengths, and their applications to nuclear waste isolation. *Applied Geochemistry*, 23, 1634–1659.

MANUSCRIPT RECEIVED OCTOBER 23, 2009

MANUSCRIPT ACCEPTED JUNE 18, 2010

MANUSCRIPT HANDLED BY NITA SAHAI